Investigation on solid solubility and magnetism of the non-stoichiometric compound Fe_3Se_4

S. Li,[1] S.F. Jin,[2] J. Ji,[1] Z.N. Guo,[1] and W.X. Yuan[1,a)]
[1]*Department of Chemistry, School of Chemical and Biological Engineering, University of Science and Technology Beijing, Beijing 100083, P. R. China*
[2]*Beijing National Laboratory for Condensed Matter Physics, Institute of Physics, Chinese Academy of Sciences, Beijing 100190, P. R. China*

(Received 5 December 2012; accepted 18 December 2012)

In order to complete the research on the Fe–Se binary system, the phase structures with selenium contents from 50 to 60 at.% have been studied. Fe–Se binary samples used in this study were prepared by the high-temperature solid-state reaction method, and the phase structure of each sample was determined by powder X-ray diffraction. The solid solubility of the Fe_3Se_4 phase was determined to be from 56.1 to 57.6 at.% Se based on the values of unit-cell parameters. Magnetic properties of the samples were also studied. © *2013 International Centre for Diffraction Data.*
[doi:10.1017/S0885715612001030]

Key words: Fe_3Se_4, powder X-ray diffraction, phase diagram, magnetic property

I. INTRODUCTION

After the superconductivity of β-FeSe was discovered by Hsu *et al.* (2008), substantial efforts have been made to design new superconducting materials based on this non-toxic layered compound (Margadonna *et al.*, 2009; Oyler *et al.*, 2009; Patel *et al.*, 2009; Williams *et al.*, 2009; Guo *et al.*, 2010; Jung *et al.*, 2010). A large number of superconducting materials have been made by doping or intercalating another component into this binary system. Up to now, the highest superconducting transition temperature of the FeSe-based materials was reported to be above 48.7 K for $K_{0.8}Fe_{1.7}Se_2$ by Sun *et al.* (2012). However, the superconducting phase in this material is still in dispute. Furthermore, the superconducting mechanism of the FeSe-based materials has not yet been reported.

Phase diagram plays a major role in designing materials and in understanding their physical and chemical properties (Pomjakushina *et al.*, 2009). As the foundation of FeSe-based materials, the Fe–Se binary system should be completely studied. The binary phase information can be extrapolated into a multi-component system, and it can also be used to calculate the thermodynamic properties, such as the energies of formation of the defects in the superconducting β-FeSe compound. There are several publications which have reported the phase information on the Fe–Se binary system (Hirone and Chiba 1956; Dutrizac *et al.*, 1968; Svendsen, 1972). Schuster *et al.* (1979) studied the entire system by isopiestic methods and X-ray analysis, and they assessed the previous literature and reported a complete phase diagram for the Fe–Se binary system. Two compounds, FeSe and $FeSe_2$ in the iron-rich portion and the selenium-rich portion, respectively, were confirmed by Schuster *et al.* (1979). The phase structures with the selenium contents from 51.5 to 58.5 at.%, which are the most complicated part of this binary system and named "$Fe_{1-x}Se$ phase" in the literature, were also determined in their work. Three non-stoichiometric compounds (hexagonal-δ and monoclinic-γ and -γ') were reported in this range, and the solid-solution ranges at 552°C were presented. However, Katayama *et al.* (1990) re-studied this "$Fe_{1-x}Se$ phase" (from 50 to 58.3 at.% Se) in the lower-temperature region at 300 and 400°C by X-ray and DTA measurements and presented results different from those reported by Schuster *et al.* (1979) in the range of 50–60 at.% Se. Another compound, Fe_7Se_8 was found in the lower temperature range. However, the monoclinic-γ' phase was not observed by Katayama *et al.* (1990) and another monoclinic phase γ was named Fe_3Se_4 and showed a totally different solid-solution range. Based on these two works, Okamoto (1991) evaluated this binary-phase diagram (shown in Figure 1), but since there was no conformity, the selenium-rich boundary of monoclinic-γ was drawn as a dashed line. Table I presents the names and the solid-solution ranges of Fe_3Se_4 reported in different previous works. Since the phase information before 1979 was all obtained in the higher-temperature range above 400°C, the results at the lower-temperature range from Katayama *et al.* (1990) need to be re-examined. Furthermore, detailed work should also be done to determine the correct solid-solution range of the monoclinic Fe_3Se_4 phase.

The magnetic properties of iron selenides can be very sensitive to their compositions. The magnetism of iron selenides was first studied by Hirone and Chiba (1954), who reported that the Curie temperature of Fe_3Se_4 is 303 K. Terzieff and Komamk (1978) also measured the magnetic properties of the compounds in the Fe–Se system and found that Fe_3Se_4 is ferrimagnetic with a different Curie temperature of 338 K. The disagreement between the results obtained by Hirone and Chiba (1954) and Terzieff and Komamk (1978) can be due to different compositions they measured in the solid-solution range.

a)Author to whom correspondence should be addressed. Electronic mail: wenxiayuan20@yahoo.cn

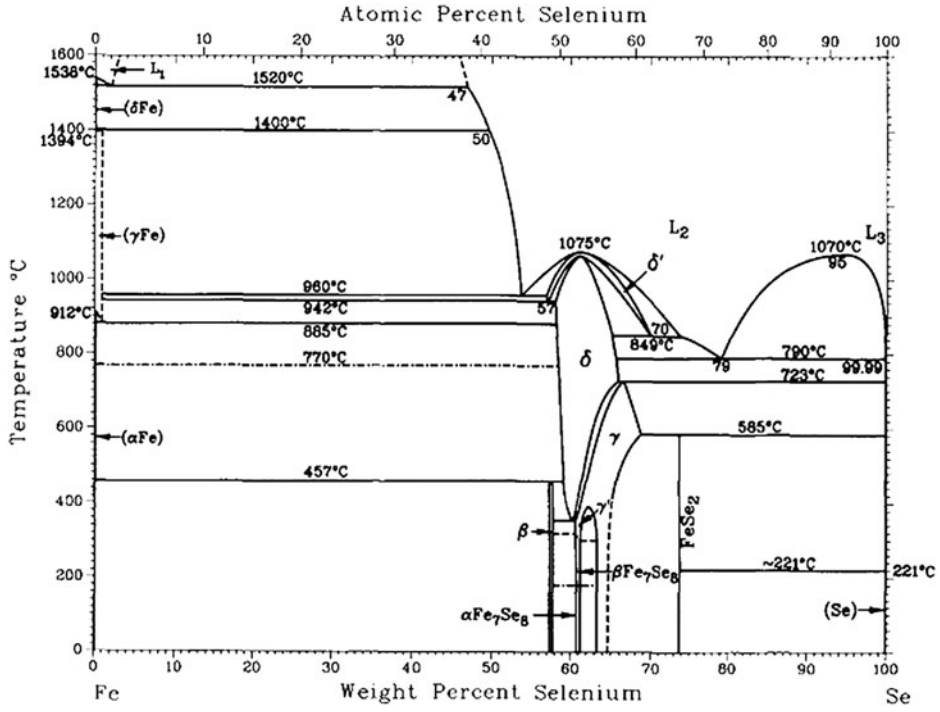

Figure 1. Phase diagram of the Fe–Se binary system by Okamota (1991).

In order to resolve the differences in the Fe–Se binary system, the phase relation of 50–60 at.% Se, the solid-solution range of Fe_3Se_4 and the magnetic properties of Fe_3Se_4 with different compositions have been examined in this work. Powder X-ray diffraction (PXRD) was carried out to obtain the phase information, and on the basis of unit-cell parameters (Grain, 1967), the solid-solution range of Fe_3Se_4 has been determined. An inductively coupled plasma-atomic emission spectrometry (ICP-AES) was used to check the chemistry compositions of the samples. Finally, a physical property measurement system (PPMS) was used to measure the magnetic properties of the Fe_3Se_4 samples.

II. EXPERIMENTAL

All samples were prepared by solid-state reaction. The pure powders of Fe (99.99%) and Se (99.95%), which are the products of China National Accord Medicines Corporation, were mixed and ground in an agate mortar, cold-pressed into disks (10 mm in diameter) with 200 kg cm^{-2} uniaxial stress and sealed in a quartz tube under vacuum. All samples were heated at 1000°C for 3 days and cooled down to room temperature in the furnace with the power switched off to get the phases in the low temperature range. A part of each sample was used for the PXRD measurement and the other part was comminuted, sealed in the quartz tube again under vacuum and re-heated at 400°C for 7 days before cooling down, to check the phase equilibrium in the sample.

PXRD data used for phase identification were collected at room temperature on a PANalytical diffractometer (X'Pert PRO MRD) equipped with Cu$K\alpha$ radiation ($\lambda = 1.5418$ Å) operating at 40 kV and 40 mA and a diffracted-beam graphite monochromator in a reflection mode ($2\theta = 10$–$80°$, step = $0.017°2\theta$, and scan speed = 5 s per step).

For precise unit-cell parameter determination, a NIST standard reference material 640 Si powder standard sample was used to calibrate the wavelength and diffractometer. The Co$K\alpha$ radiation ($\lambda = 1.7903$ Å) at 40 kV and 30 mA with a diffracted-beam graphite monochromator was used in a reflection mode ($2\theta = 5$–$135°$, step = $0.017°2\theta$, and scan speed = 20 s per step).

Magnetic susceptibility measurements were carried out using a Quantum Design PPMS magnetometer in the temperature range of 10–380 K and at a magnetic field of 0.2 T. Approximately 20–40 mg of the material was weighed accurately into a gelatin capsule. Measurements of the susceptibility were made on warming after cooling in zero field (zero field-cooled (ZFC)).

TABLE I. The solid-solution ranges of Fe_3Se_4 reported in the literature.

The literature	Phase name	Solution range (at.% Se)
Schuster *et al.* (1979)	γ	56.4–58.5
Katayama *et al.* (1990)	Fe_3Se_4	55.1–56.4
Okamota (1991)	γ	55.4–56.8

III. RESULTS AND DISCUSSION

A total of 16 samples with selenium contents from 50 to 60 at.% were investigated by PXRD. The phase composition was obtained with the first part of each sample, and PXRD was carried out again to measure the other part after the second heat treatment. XRD patterns from two parts of the samples were compared and no significant changes could be observed, which verify the equilibrium of the phases in our samples. The phase compositions of the samples in the low temperature range are listed in Table II. It can be seen that the Fe_7Se_8 phase appeared in our work, which agrees with that reported

https://doi.org/10.1017/S0885715612001030 Published online by Cambridge University Press

TABLE II. Phase compositions of the samples with selenium contents between 50 and 60 at.%.

Nominal selenium content (at.%)	Phase compositions
50.0	$FeSe + Fe_7Se_8$
51.0	$FeSe + Fe_7Se_8$
52.0	$FeSe + Fe_7Se_8$
53.0	Fe_7Se_8
54.0	Fe_7Se_8
55.0	$Fe_7Se_8 + Fe_3Se_4$
55.5	$Fe_7Se_8 + Fe_3Se_4$
56.0	$Fe_7Se_8 + Fe_3Se_4$
56.5	Fe_3Se_4
57.0	Fe_3Se_4
57.5	Fe_3Se_4
58.0	Fe_3Se_4
58.5	$Fe_3Se_4 + FeSe_2$
59.0	$Fe_3Se_4 + FeSe_2$
59.5	$Fe_3Se_4 + FeSe_2$
60.0	$Fe_3Se_4 + FeSe_2$

by Katayama *et al.* (1990), who found that the Fe_7Se_8 phase can be stable only at temperatures below 320°C. This also suggests that the phase equilibrium in our samples reached below 320°C.

In order to obtain accurate unit-cell parameters of Fe_3Se_4, ten samples around the Fe_3Se_4 solid solution were analyzed with PXRD in a reflection mode ($2\theta = 5$–$135°$, step = 0.017° 2θ, and scan speed = 20 s per step). Co$K\alpha$ radiation was used to avoid possible Fe fluorescence and to increase the resolution of the diffraction data. Moreover, a Si standard was used to calibrate the wavelength and diffractometer. XRD patterns of the samples within the 55.3–59.7 at.% Se nominal composition range are shown in Figure 2. It can be seen that within the nominal composition range of 55.3–55.7 at.% Se [Figure 2(a)], the intensities of peaks belonging to Fe_7Se_8 decrease with increasing Se content. Although the majority of Fe_7Se_8 peaks overlapped with those from Fe_3Se_4, the peak near 60°2θ can serve as a reliable indicator of the existence of Fe_7Se_8. In the patterns of the composition range between 57 and 57.8 at.% Se as shown in Figure 2(b), all the observed diffraction peaks can be indexed by a monoclinic cell, no impurity peaks arising from either the Fe_7Se_8 or $FeSe_2$ phase can be observed. The patterns are quite consistent with each other except that the position of peaks was shifted slightly to the right side with increasing Se content. For samples with nominal Se contents higher than 58.5 at.%, a considerable amount of $FeSe_2$ impurity appeared in the patterns [Figure 2(c)], indicating that the samples are within the Fe_3Se_4 and $FeSe_2$ two-phase region.

In order to obtain accurate chemical compositions of the samples, ICP-AES was used to measure the actual compositions of the five samples in the single-phase region, and the results are shown in Table III. It should be noted that the compositions of Se were smaller than the nominal compositions, which could be due to the volatility of selenium. The unit-cell parameters of these ten samples are also listed in Table III. The parameters (a, b, c, and β) of Fe_3Se_4 with different compositions are shown in Figure 3. It can be seen that in the Fe_3Se_4 single-phase region the monoclinic unit cell (space group $I2/m$) of Fe_3Se_4 decreases with increasing Se content: the a-axis from 6.2088 to 6.182 Å, the b-axis from 3.5383 to 3.5188 Å, and the c-axis from 11.318 to

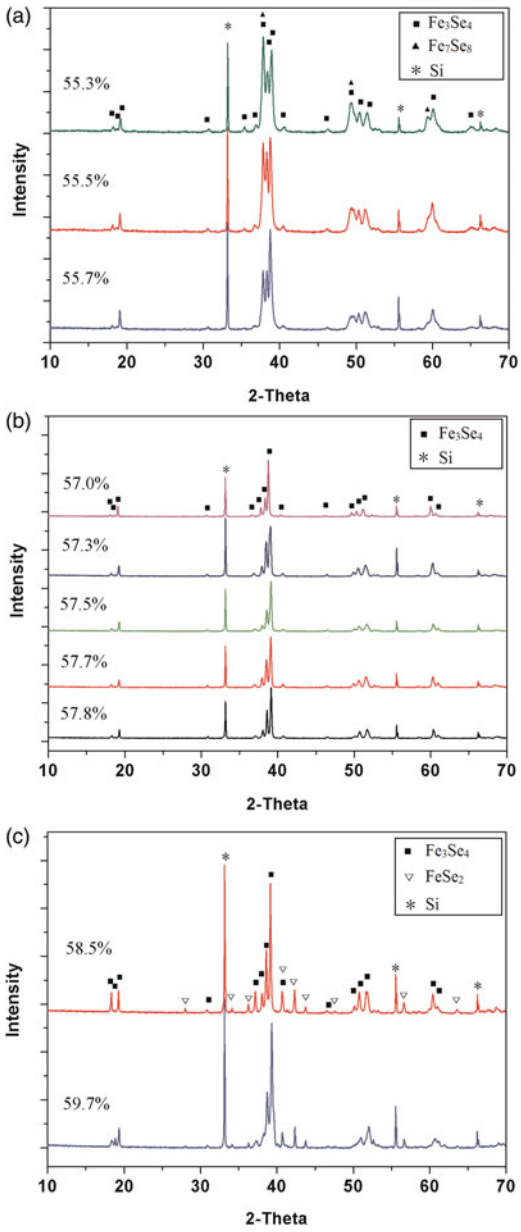

Figure 2. X-ray diffraction patterns of samples with different compositions in (a) the two-phase region: Fe_7Se_8+Fe_3Se_4, (b) the Fe_3Se_4 single-phase region, and (c) the two-phase region: $Fe_3Se_4 + FeSe_2$.

11.239 Å. It can be observed that with rising Se content, the vacancies of the iron atom are increased, which can be responsible for slightly reduced unit cells. The parameters in the two-phase regions basically remain unchanged, which agrees with the phase rule. The unit-cell volumes of Fe_3Se_4 with different compositions are plotted in Figure 4 and a linear dependence of the volume with the Se content is observed for the five samples within the single-phase region, which agrees well with Vegard's law. Unit-cell volumes of Fe_3Se_4 within the two-phase regions are also given in Figure 4, and for those samples, two horizontal lines are subsequently fitted. The solid-solution range of Fe_3Se_4, determined from the two crossing points, is from 56.1 to 57.6 at.% Se. Compared with the results from the literature in Table I, it is clear that the results from Schuster *et al.* (1979) are more reasonable. The reason for the deviation in the 1979 work could be due to the use of nominal compositions in their research.

https://doi.org/10.1017/S0885715612001030 Published online by Cambridge University Press

TABLE III. The values of unit-cell parameters of Fe_3Se_4 in the single-phase region and the adjacent two-phase regions.

x^n_{Se} (at.%)	x_{Se} (at.%)	a (Å)	b (Å)	c (Å)	β (°)	V (Å^3)
Two-phase region (Fe_7Se_8+Fe_3Se_4)						
55.3		6.219(4)	3.543(2)	11.333(7)	91.65(5)	249.61
55.5		6.210(3)	3.544(2)	11.343(5)	91.67(4)	249.53
55.7		6.220(2)	3.542(2)	11.333(6)	91.65(4)	249.58
Single-phase region (Fe_3Se_4)						
57.0	56.3	6.2088(18)	3.5383(16)	11.318(4)	91.65(2)	248.53
57.3	56.9	6.1887(8)	3.5289(7)	11.276(2)	91.924(18)	246.12
57.5	57.1	6.184(3)	3.526(2)	11.243(5)	91.86(4)	245.02
57.7	57.0	6.1873(8)	3.5249(7)	11.267(2)	91.917(14)	245.52
57.8	57.3	6.182(2)	3.5188(18)	11.239(4)	91.95(3)	244.34
Two-phase region (Fe_3Se_4+$FeSe_2$)						
58.5		6.173(3)	3.517(2)	11.197(6)	91.76(3)	242.98
59.7		6.175(4)	3.516(2)	11.198(5)	91.75(4)	243.01

x^n_{Se}: the nominal composition of Se.
x_{Se}: the composition of Se from the ICP-AES measurement.

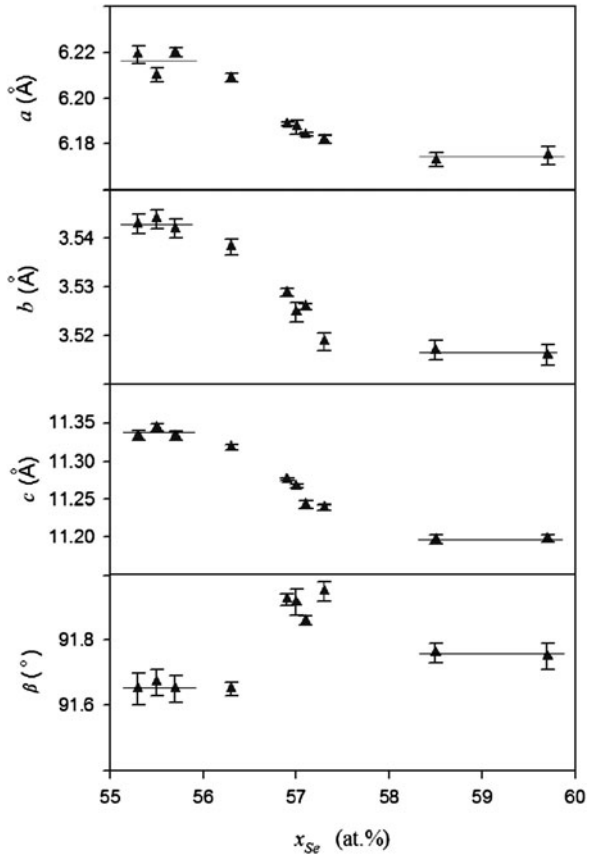

Figure 3. Unit-cell parameters (a, b, c, and β) of Fe_3Se_4 with different compositions.

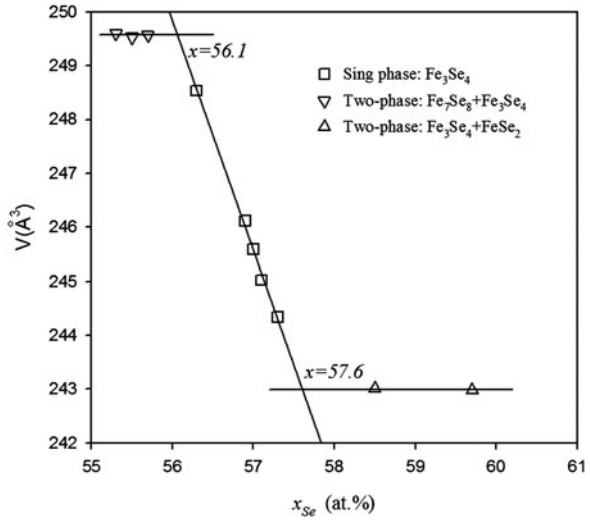

Figure 4. Variation of the unit-cell volume with the selenium content, and the solid-solution range determined from the unit-cell volume.

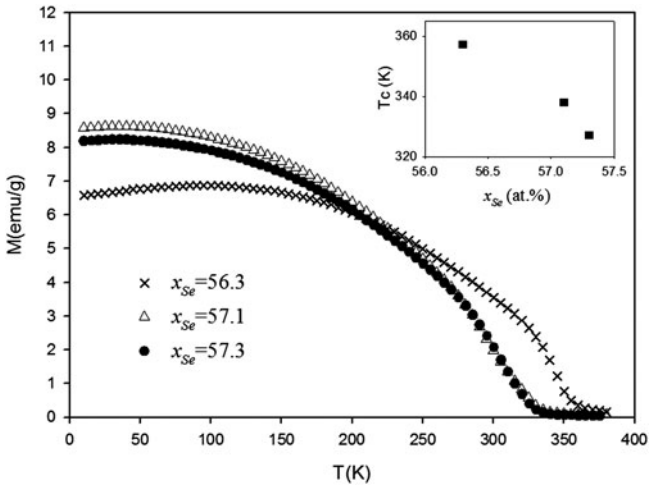

Figure 5. *M–T* curves obtained by the magnetic measurement, and the Curie temperatures calculated from the *M–T* curves.

The thermomagnetic curves of three samples with 56.3, 57.1, and 57.3 at.% Se contents are plotted in Figure 5 and the Curie temperatures calculated from the curves are shown in Table IV and are also plotted in the inset of Figure 4. Ferrimagnetism is observed from all three samples, which agrees with the work reported by Terzieff and Komamk (1978). Specifically, the Curie temperature at 57.1 at.% Se (338 K) is the same as Terzieff's results. Compared with the other compositions, it can be seen that the Curie temperature decreases with increasing Se content in the solution range of Fe_3Se_4. This trend can be attributed to an increase in non-magnetic selenium ions with increasing Fe vacancies, which weaken the interaction between the magnetic iron ions and reduce the Curie temperature.

https://doi.org/10.1017/S0885715612001030 Published online by Cambridge University Press

TABLE IV. Curie temperatures of Fe_3Se_4 with different Se contents.

x_{Se} (at.%)	56.3	57.1	57.3
Curie temperature T_c (K)	357.2	338.1	327.2

x_{Se}: the composition of Se from the ICP-AES measurement.

IV. CONCLUSION

In this work, the crystalline phases of the Fe–Se binary system with selenium contents from 50 to 60 at.% were studied by XRD and two non-stoichiometric compounds (hexagonal-Fe_7Se_8 and monoclinic-Fe_3Se_4) have been observed. The solid solubility of the Fe_3Se_4 phase has been determined based on the values of unit-cell parameters, which is from 56.1 to 57.6 at.% of selenium content. The results were compared with those from the previous literature. The thermo-magnetic curves of three samples with 56.3, 57.1, and 57.3 at.% Se were measured. Ferrimagnetism was obtained for all three samples and the Curie temperature in the Fe_3Se_4 solid solution was calculated and found to decrease with increasing Se content.

ACKNOWLEDGEMENTS

Financial support from the National Natural Science Foundation of China (numbers 50772012,51172025 and 50972010) and the Fundamental Research Funds for the Central Universities (number FRF-TP-09-021B) is gratefully acknowledged. The authors also thank Yanping Xu for her help with PXRD measurements.

Dutrizac, J. E., Janjua, M. B. I., and Tognri, J. M. (**1968**). "Phase studies on the iron–selenium system," Can. J. Chem. **46**, 1171–1174.

Grain, C. F. (**1967**). "Phase relations in the ZrO_2–MgO system," J. Am. Ceram. Soc. **50**, 288–290.

Guo, J. G., Jin, S. F., Wang, G., Wang, S. C., Zhu, K. X., Zhou, T. T., He, M., and Chen, X. L. (**2010**). "Superconductivity in the iron selenide $K_xFe_2Se_2(0 \le x \le 1.0)$," Phys. Rev. B. **82**, 180520.

Hirone, T. and Chiba, T. (**1956**). "The magnetic properties of $FeSe_x$ with the NiAs structure," J. Phys. Soc. Japan **11**, 666–670.

Hirone, T., Maeda, S., and Tsuya, N. (**1954**). "On the ferrimagnetism of iron selenides," J. Phys. Soc. Japan **9**, 496–499.

Hsu, F. C., Luo, J. Y., Yeh, K. W., Chen, T. K., Huang, T. W., Phillip, Wu, M., Lee, Y. C., Huang, Y. L., Chu, Y. Y., Yan, D. C., and Wu, M. K. (**2008**). "Superconductivity in the PbO-type structure α-FeSe," Proc. Natl. Acad. Sci. U.S.A. **105**, 14262–14264.

Jung, S. G., Lee, N. H., Choi, E. M., Kang, W. N., Lee, S., Hwang, T., and Kin, D. H. (**2010**) "Fabrication of $FeSe_{1-x}$ superconducting films with bulk properties," Physica C **470**, 1977–1980.

Katayama, S., Uoda, Y., and Kosuge, K. (**1990**). "Phase diagram and order–disorder transition of vacancies in the Cr–Se and Fe–Se systems," Mater. Res. Bull. **25**, 913–922.

Margadonna, S., Takabayashi, Y., Ohishi, Y., Mizuguchi, Y., Takano, Y., Kagayama, T., Nakagawa, T., Takata, M., and Prassides, K. (**2009**). "Pressure evolution of the low-temperature crystal structure and bonding of the superconductor FeSe ($T_c = 37$ K)," Phys. Rev. B **80**, 064506.

Okamoto, H. (**1991**). "The Fe–Se (iron–selenium) system," J. Phase Equilib. **12**, 383–389.

Oyler, K. D., Ke, X., Sines, I. T., Schiffer, P., and Schaak, R. E. (**2009**). "Chemical synthesis of two-dimensional iron chalcogenide nanosheets: FeSe, FeTe, Fe(Se, Te), and $FeTe_2$," Chem. Mater. **21**, 3655–3661.

Patel, U., Hua, J., Yu, S. H., Avci, S., Xiao, Z. L., Claus, H., Schlueter, J., Vlasko-Vlasov, V. V., Welp, U. and Kwok, W. K. (**2009**). "Growth and superconductivity of $FeSe_x$ crystals," Appl. Phys. Lett. **94**, 082508.

Pomjakushina, E., Conder, K., Pomjakushin, V., Bendele, M., and Khasanov, R. (**2009**). "Synthesis crystal structure, and chemical stability of the superconductor $FeSe_{1-x}$," Phys. Rev. B. **80**, 024517.

Schuster, W., Mikler, H., and Komarek, K. L. (**1979**). "Transition metal–chalcogen systems, VII: the iron–selenium phase diagram," Monatsh. Chem. **110**, 1153–1170.

Sun, L. L., Chen, X. J., Guo, J., Gao, P. W., Huang, Q. Z., Wang, H. D., Fang, M. H., Chen, X. L., Chen, G. F., Wu, Q., Zhang, C., Gu, D. C., Dong, X. l., Wang, L., Yang, K., Li, A. G., Dai, X., Mao, H. K., and Zhao, Z. X. (**2012**). "Re-emerging superconductivity at 48 Kelvin in iron chalcogenides," Nat. Phys. **483**, 67–69.

Svendsen, S. R. (**1972**). "Decomposition pressures and standard enthalpy of formation of iron selenides FeSe, Fe_7Se_8, Fe_3Se_4, and $FeSe_2$," Acta Chem. Scand. **26**, 3757–3774.

Terzieff, P., and Komamk, K. L. (**1978**). "The paramagnetic properties of iron selenides with NiAs-type structure," Monatsh. Chem. **109**, 651–659.

Williams, A. J., McQueen, T. M., and Cava, R. J. (**2009**). "The stoichiometry of FeSe," Solid State Commun. **149**, 1507–1509.